Permeability Description by Characteristic Length, Tortuosity, Constriction and Porosity

Carl Fredrik Berg

Abstract In this article we investigate the permeability of a porous medium as given in Darcy's law. The permeability is described by an effective hydraulic pore radius in the porous medium, the fluctuation in local hydraulic pore radii, the length of streamlines, and the fractional volume conducting flow. The effective hydraulic pore radius is related to a characteristic hydraulic length, the fluctuation in local hydraulic radii is related to a constriction factor, the length of streamlines is characterized by a tortuosity, and the fractional volume conducting flow from inlet to outlet is described by an effective porosity. The characteristic length, the constriction factor, the tortuosity, and the effective porosity are thus intrinsic descriptors of the pore structure relative to direction. We show that the combined effect of our pore structure description fully describes the permeability of a porous medium. The theory is applied to idealized porous media, where it reproduces Darcy's law for fluid flow derived from the Hagen–Poiseuille equation. We also apply this theory to full network models of Fontainebleau sandstone, where we show how the pore structure and permeability correlate with porosity for such natural porous media. This work establishes how the permeability can be related to porosity, in the sense of Kozeny–Carman, through fundamental and well-defined pore structure parameters: characteristic length, constriction, and tortuosity.

Keywords Porous media · Permeability · Tortuosity · Characteristic length · Kozeny–Carman equation

1 Introduction

Understanding the process of flow through porous media is of great importance in many fields, including petroleum engineering and hydrology. Slow viscous fluid flow in porous

C. F. Berg (✉)
Statoil R&D Center, Arkitekt Ebbels veg 10, Rotvoll, 7053 Trondheim, Norway
e-mail: cfbe@statoil.com

media is traditionally described by Darcy's law, a proportional relation that links the fluid discharge Q to an applied piezometric head (hydraulic head) difference Δh:

$$k = -\frac{Q\mu\Delta s}{A\rho g\Delta h}, \tag{1}$$

where A is the cross-sectional area of the porous medium, Δs is the length of the porous medium in direction of applied head difference, μ is the constant fluid viscosity, ρ is the constant fluid density, g is acceleration due to gravity, and k is a constant for the porous medium called (intrinsic) permeability (Darcy 1856; Bear 1988; Dullien 1992). For simplicity, $\rho g h$ will also be called the piezometric head throughout this article.

A fundamental question in flow through porous media is how the permeability k can be related to the porosity ϕ through well-defined parameters of the pore structure. A well-known relation of this kind is the semi-empirical Kozeny–Carman equation. It was first proposed by Kozeny (1927) as

$$k \propto \tau\frac{\phi^3}{(1-\phi)^2}d_{\mathrm{w}}^2, \tag{2}$$

where d_{w} is an effective grain size, and τ is a tortuosity of the porous medium describing the relative difference between the microscopic (interstitial) head gradient along the streamline and the macroscopic head gradient. Kozeny derived his equation assuming that the porous medium could be viewed as a bundle of streamtubes (Kozeny 1927).

Carman noted that linking the microscopic fluid velocity to the Darcy velocity for the porous medium involves scaling with the factor τ (Carman 1937). Carman therefore modified Kozeny's Eq. (2) by multiplying with the tortuosity τ (Carman 1937):

$$k \propto \tau^2\frac{\phi^3}{(1-\phi)^2}d_{\mathrm{w}}^2. \tag{3}$$

For a monodisperse sphere pack we have $d_{\mathrm{w}} = 6(1-\phi)/S_0$, where S_0 is the specific surface area (Kozeny 1927). This leads to a more general form of the Kozeny–Carman equation:

$$k = c_0\tau^2\frac{\phi^3}{S_0^2} = c_0\tau^2 r_{\mathrm{h}}^2\phi, \tag{4}$$

here $r_{\mathrm{h}} = \phi/S_0$ is the (mean) hydraulic radius, and c_o is a coefficient called Kozeny's constant (Kozeny 1927; Carman 1937; Bear 1988; Dullien 1992).

The hydraulic radius r_{h} is assumed to represent an effective pore radius of the porous medium. It is a purely geometric length which does not take into account the effect on permeability from pore size variation or connectivity. Others have proposed length scales more suitable for permeability description, among these the smallest pore along the most conductive percolating pathway (Katz and Thompson 1986), nuclear magnetic resonance relaxation time (Banavar and Schwartz 1987), or grain size distribution (Berg 1970). Johnson et al. (1986) suggested that a length by weighting with the electric field, thereby related to (electrical) transport and thus a dynamical length in contrast to the geometrical hydraulic radius r_{h}. This length has been shown to be a better permeability descriptor than the hydraulic radius r_{h} (Schwartz et al. 1993); however, there is no fixed relation between electrical conductance and fluid flow (Saeger et al. 1991). A dynamical length linked to fluid flow instead of electrical conductance was introduced in Bear and Bachmat (1967). This length was derived from the microscopic hydraulic conductance (Bear and Bachmat 1967; Bear 1988), thus, descriptive of fluid flow in porous media.

For a porous medium, the (hydraulic) tortuosity is a measure of the microscopic flows deviation from the direction of the applied piezometric head difference, reflected by the length of the microscopic streamlines (Bear 1988; Dullien 1992; Adler 1992). Tortuosity has been defined as $\Delta s / s_e$, where Δs is the length of the porous medium in the direction of applied piezometric head difference, and s_e is the effective streamline length (Bear 1988; Koponen et al. 1996). There is ambiguity associated with the derivation of s_e (Bear 1988; Koponen et al. 1996); however, most formulations are a weighted average of the streamline lengths (Duda et al. 2011).

Furthermore, the constricting and expanding nature of pore channels converges and diverges the streamlines, which leads to variation in fluid velocity along the streamlines and decrease the permeability. This effect has been treated for simplified porous media (Dullien 1992), and for more complex material the standard deviation of the cross-sectional area has been used as an estimate (Schopper 1966), while for electrical conductance the effect of pore channel variation has been described in general (Berg 2012). We follow Dullien (1992) and use the term constriction factor to account for this porous medium property. Note that the term constrictibility is common when considering effective diffusion in porous media, see e.g., Brakel and Heertjes (1974). The effect on transport from constrictions is frequently lumped together with the effect from tortuosity, see e.g., Schwartz et al. (1993), Bear and Bachmat (1967), Bear (1988). However, the pore structure effect on permeability from these two distinct geometrical properties can be separated for any porous medium, as shown in this article.

The (geometrical) porosity $\phi = \Omega / V$ is the fraction of pore space Ω in the porous medium of total volume V. The pore space Ω is sometimes interpreted as the connected pore space; thus, both the permeability and porosity vanish at a percolation threshold at a finite geometrical porosity (Mavko and Nur 1997). Other authors have also excluded dead-end pores (Bear 1988; Guo 2012), or considered an effective porosity based on the streamlines connected both to the inlet and the outlet of the porous medium (Duda et al. 2011; Koponen et al. 1997).

A large body of literature exists on the relation between macroscopic transport properties and pore structure; the interested reader is referred to Dullien (1992) and Bear (1988) for reviews of numerous relations. The recent progress in computing and imaging provides tools for advances on the topic. A number of methods for statistically (Adler et al. 1990; Yeong and Torquato 1998; Jiao et al. 2009) or process-based (Øren and Bakke 2002) reconstruction of three-dimensional porous media from two-dimensional thin section images have been proposed. Advances in micro-computed tomography (mCT) have made it possible to directly image many types of natural porous media with sufficient resolution to represent the three-dimensional pore structure (Schwartz et al. 1994; Arns et al. 2001). For flow and transport simulations network analogs have been widely used to represent the pore space (Fatt 1956; Blunt 2001; Øren et al. 1998), while the full microscopic pressure and velocity fields can also be computed for both idealized models (Lemaitre and Adler 1990; Schwartz et al. 1993; Zhang and Knackstedt 1995) and for natural porous media such as reservoir rocks (Arns et al. 2001; Mostaghimi et al. 2013).

The aim of this work is to derive a comprehensive relation for porous media between the permeability and porosity from detailed pore structure information. In contrast with existing relations the permeability will be fully defined by separable descriptors of the pore structure without introducing free parameters or constants. In Sect. 2 we introduce a microscopic permeability factor which describes the local contribution to the effectiveness of the pore space to conduct fluid flow. This permeability factor is decomposed into streamlines of the fluid flow, and further factorized into distinct contributions from characteristic length, constriction,

and tortuosity in Sect. 3. In Sect. 4 we integrate the characteristic length, constriction, and tortuosity from individual streamlines into effective parameters, all pore structure descriptors. In Sect. 5 we use the Hagen–Poiseuille equation to demonstrate our approach on idealized porous media, while the methodology is applied to network analogs of Fontainebleau sandstone data in Sect. 6.

2 Microscopic (Interstitial) Permeability

Consider a porous medium V of length Δs in direction of an applied piezometric head difference Δh, consisting of matrix and pore space $\Omega \subset V$ filled with an incompressible fluid. At the microscopic (interstitial) scale, a slow (creeping) flow is governed by the Stokes equation supplemented by the continuity equation:

$$\mu \nabla^2 \mathbf{u} = \rho g \nabla h, \tag{5a}$$

$$\nabla \cdot \mathbf{u} = 0, \tag{5b}$$

where $\mathbf{u}$ is the microscopic fluid velocity, and h is the microscopic piezometric head (Dullien 1992; Bear 1988; Adler 1992). In the following we will refer to Eqs. (5) simply as the Stokes equations. Throughout this article the fluid flow is assumed to be governed by the Stokes equations. There are no time derivative terms in the Stokes equations; hence a constant piezometric head difference Δh implies a steady-state flow.

Let $\mathbb{S}$ denote the set of all streamlines $\mathcal{S}$ connected both to the inlet and the outlet of the porous medium, and let $\Omega_s = \{x \in \mathcal{S} \in \mathbb{S}\}$ be the subset of Ω where the fluid flows from inlet to outlet. The effective porosity is $\phi_s = \Omega_s / V$ (Koponen et al. 1997; Duda et al. 2011). Due to the linearity of the Stokes equations, the streamlines $\mathcal{S}$ are independent of the magnitude of applied piezometric head drop Δh, and the constants ρ and μ, thus, Ω_s and ϕ_s are only dependent on pore structure and direction of the applied piezometric head drop. Note that for dead-end pores we might have pore space that is not in Ω_s, still the fluid velocity might be non-zero, called reentrant flow in Duda et al. (2011).

In our system the piezometric head difference $-\rho g \Delta h$ is the potential that drives the fluid through the porous medium, hence the rate of applied energy is $-\rho g \Delta h Q$. The potential driving the microscopic fluid flow is the piezometric head $\rho g h$, and the rate of work done by this piezometric head potential is given by $-\rho g \nabla h \cdot \mathbf{u}$.

Applying the divergence theorem, and invoking that the fluid velocity $\mathbf{u}$ is a solenoidal vector field from the continuity equation Eq. (5b), we obtain

$$\int_{\Omega_s} \rho g \nabla h \cdot \mathbf{u} dV = \int_{\Omega_s} \rho g \nabla h \cdot \mathbf{u} + \rho g h (\nabla \cdot \mathbf{u}) dV$$
$$= \int_{\Omega_s} \nabla \cdot (\rho g h \mathbf{u}) \, dV = \int_{\delta \Omega_s} \rho g h \mathbf{u} \cdot \mathbf{n} dS$$
$$= \rho g (h_{\text{out}} Q - h_{\text{in}} Q) = \rho g \Delta h Q, \tag{6}$$

where $\mathbf{n}$ is the outward pointing unit normal field of the boundary $\delta \Omega_s$, h_{in} is the piezometric head at inlet, and h_{out} the head at outlet. Here we use that $\mathbf{u} \cdot \mathbf{n} = 0$ except at inlet and outlet.

The permeability as given by Darcy's law in Eq. (1) can then be expressed as follows:

$$k = -\frac{Q \mu \Delta s}{A \rho g \Delta h} = \phi_s \frac{1}{\Omega_s} \int_{\Omega_s} -\mu \rho g \nabla h \cdot \mathbf{u} \left(\frac{\Delta s}{\rho g \Delta h} \right)^2 dV. \tag{7}$$

We will denote the integrand in Eq. ([7](#)) as the microscopic permeability factor:

$$\kappa = -\mu\rho g \nabla h \cdot \mathbf{u} \left(\frac{\Delta s}{\rho g \Delta h}\right)^2. \tag{8}$$

The microscopic permeability factor κ is then the rate of work done by the piezometric head potential $-\rho g \nabla h \cdot \mathbf{u}$ multiplied by the factor $\mu \Delta s^2/(\rho g \Delta h)^2$; however, it is a constant only dependent on the pore space $\Omega \subset V$ and the direction of the applied head difference Δh, in contrast to $-\rho g \nabla h \cdot \mathbf{u}$.

We derive the effective permeability factor by integrating κ over Ω_s:

$$\kappa_s = \frac{1}{\Omega_s} \int_{\Omega_s} \kappa dV = -\frac{1}{\Omega_s} \mu\rho g \Delta h Q \left(\frac{\Delta s}{\rho g \Delta h}\right)^2. \tag{9}$$

Since the microscopic permeability factors κ are constants only dependent on the pore space and the direction of the applied head difference Δh, so is the macroscopic permeability factor κ_s. Moreover,

$$k = \kappa_s \phi_s. \tag{10}$$

We have thereby divided the permeability into two factors; the effective porosity ϕ_s yielding the pore space fraction where fluid flow from inlet to outlet, and the permeability factor κ_s yielding the effectiveness of the pore space Ω_s to conduct fluid flow. Both ϕ_s and κ_s are dependent on direction, leading to the anisotropy of the permeability.

Following the same arguments as above we also have

$$k = \hat{\kappa}\phi, \tag{11}$$

where

$$\hat{\kappa} = \frac{1}{\Omega} \int_\Omega \kappa dV. \tag{12}$$

This implies that

$$\int_{\Omega \setminus \Omega_s} \kappa dV = 0, \tag{13}$$

even though the permeability factor κ might be non-zero in $\Omega \setminus \Omega_s$. Hence reentrant flow does not contribute to the effective permeability factor. In the following we work with streamlines connected to inlet and outlet, thereby excluding the part of the pore space containing reentrant flow in addition to stagnant parts.

3 Streamline Decomposition

In this section, we show how the permeability factor can be decomposed onto streamlines, and furthermore how the permeability factor for each streamline can be segmented into parts describing the hydraulic conductance, the constrictions, and the tortuosity along this streamline.

We can discretize the space Ω_s into a disjoint union of simply connected spaces, such that each streamline is fully contained within one simply connected space. Using the continuity equation given by Eq. ([5b](#)), there exist scalar functions Λ and X such that $\nabla\Lambda \times \nabla X = \mathbf{u}$ (Bear 1988; Aris 1989). The scalar functions Λ and X represent two families of stream surfaces whose intersections are the streamlines.

Every point in $x \in \Omega_s$ is uniquely described by the streamline $\mathcal{S}$ passing through x, and the distance s along $\mathcal{S}$ from inlet to point x. The streamline $\mathcal{S} = \mathcal{S}(\Lambda = \lambda, X = \chi)$ is the intersection of the surfaces given by the constants λ and χ. This is similar to a Lagrangian frame of reference; however, we use distance instead of time to distinguish points on a streamline. A change of variables from the usual Cartesian coordinates (x, y, z) to the streamline coordinates (Λ, X, s) gives the Jacobian

$$\left\| \frac{\delta(\Lambda, X, s)}{\delta(x, y, z)} \right\| = (\nabla\Lambda \times \nabla X) \cdot \nabla s = \mathbf{u} \cdot \frac{\mathbf{u}}{u} = u. \tag{14}$$

By vector calculus identities we have $\mathbf{u} = \nabla\Lambda \times \nabla X = \nabla \times \Lambda\nabla X$. Using Stokes' theorem, the fluid discharge $\hat{Q}$ through a streamtube bounded by four stream surfaces represented by the constants $\lambda_1, \lambda_2, \chi_1,$ and χ_2 is then

$$\hat{Q} = \int\int_S \mathbf{u} \cdot \mathbf{n} dS = \int_{\delta S} \Lambda\nabla X \cdot \mathbf{l} ds = (\lambda_2 - \lambda_1)(\chi_2 - \chi_1), \tag{15}$$

where S is a cross section of the streamtube, and $\mathbf{l}$ is the unit tangent to the surface boundary δS. In the last equality we use that either Λ or X is constant for each of the four line segments in δS.

We can now define a permeability factor for the individual streamlines. Starting with Eq. (9) we have

$$\begin{aligned}
\kappa_s &= \frac{1}{\Omega_s} \int_{\Omega_s} \kappa dV = \frac{1}{\Omega_s} \int\int\int_{\mathcal{S}(\Lambda, X)} \frac{\kappa}{u} ds dX d\Lambda \\
&= \frac{1}{\Omega_s} \int\int\int_{\mathcal{S}(\Lambda, X)} -\mu\rho g \frac{\nabla h \cdot \mathbf{u}}{u} \left(\frac{\Delta s}{\rho g \Delta h}\right)^2 ds dX d\Lambda \\
&= \frac{1}{\Omega_s} \int_{\mathbb{S}} -\mu\rho g \Delta h \left(\frac{\Delta s}{\rho g \Delta h}\right)^2 dQ_{\mathcal{S}} = \frac{1}{\Omega_s} \int_{\mathbb{S}} \kappa(\mathcal{S}) dQ_{\mathcal{S}},
\end{aligned} \tag{16}$$

where $\kappa(\mathcal{S}) = -\mu\Delta s^2/(\rho g \Delta h)$ is the permeability factor for the streamline $\mathcal{S}$. For the fourth equality we use that $\nabla h \cdot \mathbf{u}/u = \delta h/\delta s$, and that the total head difference along a streamline is equal to the applied head difference Δh. The infinitesimal fluid discharge for the infinitesimal streamtube given by dX and $d\Lambda$ is denoted by $dQ_{\mathcal{S}}$, where $dX d\Lambda = dQ_{\mathcal{S}}$ from Eq. (15).

Note that $\kappa(\mathcal{S})$ is a constant and that

$$\kappa_s = \frac{1}{\Omega_s} \int_{\mathbb{S}} \kappa(\mathcal{S}) dQ_{\mathcal{S}} = \frac{1}{\Omega_s} \kappa(\mathcal{S}) \int_{\mathbb{S}} dQ_{\mathcal{S}} = \frac{Q}{\Omega_s} \kappa(\mathcal{S}). \tag{17}$$

Rewriting the expression for $\kappa(\mathcal{S})$, we obtain

$$\kappa(\mathcal{S}) = -\frac{\mu\Delta s^2}{\rho g \Delta h} = \left(\frac{\Delta s}{l_{\mathcal{S}}}\right)^2 \int_S -\frac{\mu u}{\rho g \nabla h \cdot \mathbf{u}} ds \left(\frac{1}{l_{\mathcal{S}}^2} \Delta h \int_S \frac{u}{\nabla h \cdot \mathbf{u}} ds\right)^{-}, \tag{18}$$

where $l_{\mathcal{S}}$ is the length of the streamline $\mathcal{S}$. In the following, we will link the permeability factor for a streamline to descriptors of the pore structure: namely, tortuosity, constriction, and hydraulic conductance; all represented in Eq. (18).

3.1 Tortuosity

The tortuosity of the streamline $\mathcal{S}$ is given by $\tau(\mathcal{S}) = \Delta s/l_{\mathcal{S}}$, i.e., the length of the porous medium divided by the length of the streamline (Bear 1988; Koponen et al. 1996). Due to the

linearity of the Stokes equations, Eqs. (5), the streamline $\mathcal{S}$ is independent of the magnitude of applied piezometric head drop Δh and the constants ρ and μ; thus, $\tau(\mathcal{S})$ is only dependent on pore structure and direction of the applied piezometric head drop.

For smaller tortuosity $\tau(\mathcal{S})$ the fluid needs to travel longer distance, and more applied head potential is expended due to transport distance. This increase in energy expenditure is reflected in the smaller factor $\tau(\mathcal{S})^2 = (\Delta s / l_{\mathcal{S}})^2$ in Eq. (18). Longer travel distance for the fluid decreases the effectiveness of the pore space to conduct flow.

3.2 Constriction Factor

For a straight circular pore channel of length L with cross-sectional area $A(x)$ at point x, the degree of variation in cross-sectional area can be measured by the constriction factor

$$C = \frac{1}{L^2} \int_0^L A(x)^2 dx \int_0^L \frac{1}{A(x)^2} dx \tag{19}$$

$$= \frac{1}{L^2} \int_0^L \frac{Q}{\rho g \nabla h(x)} dx \int_0^L \frac{\rho g \nabla h(x)}{Q} dx$$

$$= \frac{1}{L^2} \int_0^L \frac{1}{\nabla h(x)} dx \int_0^L \nabla h(x) dx, \tag{20}$$

corresponding to definitions introduced in Dullien (1992), Berg (2012). For the second equality we assume that the fluid flow is described by the Hagen–Poiseuille equation (see Eq. (33)); thus, $Q/(\rho g \nabla h(x)) \propto A(x)^2$. When the fluid is incompressible, the total discharge Q must be constant through all pore channel cross sections due to mass-balance, yielding Eq. (20). For porous media in general, the cross-sectional area $A(x)$ used in Eq. (19) is not straightforward defined. As seen in Sect. 5.4, C represents the reduction in permeability due to the variation in cross-sectional area.

Following Berg (2012) we propose a (hydraulic) constriction factor for streamline $\mathcal{S}$ by replacing the head gradient ∇h in Eq. (20) with the head derivative $\delta h / \delta s = \nabla h \cdot \mathbf{u} / u$ along the streamline:

$$C(\mathcal{S}) = \frac{1}{l_{\mathcal{S}}^2} \int_{\mathcal{S}} \frac{u}{\nabla h \cdot \mathbf{u}} ds \int_{\mathcal{S}} \frac{\nabla h \cdot \mathbf{u}}{u} ds = \frac{1}{l_{\mathcal{S}}^2} \Delta h \int_{\mathcal{S}} \frac{u}{\nabla h \cdot \mathbf{u}} ds. \tag{21}$$

As with the tortuosity $\tau(\mathcal{S})$, the constriction factor $C(\mathcal{S})$ is only dependent on pore structure and direction.

When the fluid flows through a constriction, the head derivative $\delta h / \delta s$ along the streamline increases. A large variation in pore size along the streamline then translates into a large variation in the head derivative. The constriction factor $C(\mathcal{S})$ thus relates to the constricting and expanding nature of the pore space along the streamline $\mathcal{S}$ or equivalently the converging–diverging set of streamlines around streamline $\mathcal{S}$. For a larger constriction factor $C(\mathcal{S})$ the effectiveness of the pore space to conduct flow is reduced.

3.3 Hydraulic Conductance

The microscopic hydraulic conductance is given by

$$B = -\frac{\mu u^2}{\rho g \nabla h \cdot \mathbf{u}}, \tag{22}$$

and is related to the pore size and shape, and the location in the pore (Bear and Bachmat 1967; Bear 1988). Following Eq. (16), the hydraulic conductance for a streamline $\mathcal{S}$ is

$$B(\mathcal{S}) = \int_{\mathcal{S}} B \frac{1}{u} ds = \int_{\mathcal{S}} -\frac{\mu u}{\rho g \nabla h \cdot \mathbf{u}} ds. \tag{23}$$

Observe that $B(\mathcal{S})$ represents the second term of Eq. (18). Also note that $B(\mathcal{S})$ is dependent on both the magnitude of the applied piezometric head drop $\rho g \Delta h$ and the viscosity μ, in addition to pore structure and direction of the applied head drop. This is in contrast with the hydraulic conductance B, tortuosity $\tau(\mathcal{S})$, and constriction factor $C(\mathcal{S})$, which are only dependent on pore structure and direction.

With the formulations above, Eq. (18) can now be rewritten as follows:

$$\kappa(\mathcal{S}) = \frac{B(\mathcal{S})\tau(\mathcal{S})^2}{C(\mathcal{S})}. \tag{24}$$

The permeability factor for an individual streamline is then expressed by descriptors of the pore structure.

4 Effective Permeability

In this section we show how the permeability factor κ_s can be segmented into a characteristic length, a constriction factor, and a tortuosity by averaging over the streamline values. These are strictly related to fluid flow, based on the solution of the Stokes equation inside the porous medium.

The effective hydraulic conductance is found as the volume-weighted average of the hydraulic conductance B (Bear and Bachmat 1967; Bear 1988):

$$B_{\mathrm{s}} = \frac{1}{\Omega_{\mathrm{s}}} \int_{\Omega_{\mathrm{s}}} B dV. \tag{25}$$

Since B is only dependent on pore space and direction, so is B_{s}. From

$$B_s = \frac{1}{\Omega_s} \int_{\Omega_s} B dV = \frac{1}{\Omega_s} \int_{\mathbb{S}} B(\mathcal{S}) dQ_{\mathcal{S}}, \tag{26}$$

we have a correspondence between the volume integral of B and the streamline integral of $B(\mathcal{S})$.

We define the characteristic (hydraulic) length as $L_{\mathrm{h}} = \sqrt{8B_{\mathrm{s}}}$ to represent the effective hydraulic pore radius of the porous medium. Note that the characteristic length scales linearly with the size of the porous medium, as desired for a characteristic length. As seen in Sect. 5.2, for a porous medium consisting of parallel circular tubes of radius r and length Δs, where these tubes connect the opposite sides of a cube of side-length Δs, then $L_{\mathrm{h}} = r$, and $k = \phi_{\mathrm{s}}\kappa_{\mathrm{s}} = \phi_{\mathrm{s}}B_{\mathrm{s}} = \phi_{\mathrm{s}}L_{\mathrm{h}}^2/8$ as desired for such a medium (Dullien 1992).

Consider a porous medium for which $C(\mathcal{S}) = 1$ for all streamlines $\mathcal{S}$, e.g., a single tube of constant cross-sectional area. Following Eq. (4), for such a porous medium we desire for

a tortuosity τ_s^2 to give $k = \phi_s B_s \tau_s^2$ (Dullien 1992; Bear 1988). Then $\kappa_s = B_s \tau_s^2$ by Eq. (10), thus invoking Eq. (24) gives

$$\tau_s^2 = \frac{1}{\int_{\mathbb{S}} B(\mathcal{S})dQ_{\mathcal{S}}} \int_{\mathbb{S}} \tau^2(\mathcal{S})B(\mathcal{S})dQ_{\mathcal{S}}. \tag{27}$$

Hence the tortuosity squared τ_s^2 is a weighted average of the streamline tortuosity squared. Note that the tortuosity τ_s^2 is only dependent on the pore space Ω_s and the direction of applied piezometric head drop, it is dimensionless and scale invariant.

The tortuosity is commonly formulated as a weighted average of the streamline lengths (Duda et al. 2011; Koponen et al. 1997); therefore, let the tortuosity $\hat{\tau}^\alpha = 1/\int_{\mathbb{S}} \hat{w}(\mathcal{S})dQ_{\mathcal{S}} \int_{\mathbb{S}} \tau^\alpha(\mathcal{S})\hat{w}(\mathcal{S})dQ_{\mathcal{S}}$ be another weighted average of streamline tortuosity $\tau(\mathcal{S})$, now to a power α. Consider a porous medium for which $C(\mathcal{S}) = 1$, and $\tau(\mathcal{S})$ is constant for all streamlines $\mathcal{S}$. We still want $k = \phi_s B_s \hat{\tau}^\alpha$; thus, $\hat{\tau}^\alpha = \tau_s^2$, which yields

$$\tau^\alpha(\mathcal{S}) = \frac{1}{\int_{\mathbb{S}} \hat{w}(\mathcal{S})dQ_{\mathcal{S}}} \int_{\mathbb{S}} \tau^\alpha(\mathcal{S})\hat{w}(\mathcal{S})dQ_{\mathcal{S}} = \hat{\tau}^\alpha = \tau_s^2 = \tau^2(\mathcal{S}), \tag{28}$$

therefore $\alpha = 2$. If we desire a streamline decomposition to hold for $B_s \hat{\tau}^2 = \int_{\mathbb{S}} \kappa(\mathcal{S})dQ_{\mathcal{S}}$, then $(\int_{\mathbb{S}} B(\mathcal{S})dQ_{\mathcal{S}}/\int_{\mathbb{S}} \hat{w}(\mathcal{S})dQ_{\mathcal{S}})\hat{w}(\mathcal{S}) = B(\mathcal{S})$, yielding τ_s^2 unique of the form described by $\hat{\tau}^\alpha$.

Using Eqs. (17), (24), (26) and (27), we have

$$B_s \tau_s^2 = \frac{1}{\Omega_s} \int_{\mathbb{S}} B(\mathcal{S})\tau^2(\mathcal{S})dQ_{\mathcal{S}} = \frac{1}{\Omega_s} \int_{\mathbb{S}} \kappa(\mathcal{S})C(\mathcal{S})dQ_{\mathcal{S}} = \kappa_s \frac{1}{Q} \int_{\mathbb{S}} C(\mathcal{S})dQ_{\mathcal{S}}. \tag{29}$$

By factoring out the hydraulic conductance B_s and tortuosity τ_s^2, the remaining contribution to the permeability factor κ_s is

$$C_s = \frac{1}{Q} \int_{\mathbb{S}} C(\mathcal{S})dQ_{\mathcal{S}}, \tag{30}$$

where C_s is denoted the (hydraulic) constriction factor. The constriction factor is also only dependent on the pore space Ω_s and direction; it is dimensionless and scale invariant. While the hydraulic conductance represents an effective hydraulic pore radius, the constriction factor represents the fluctuation in hydraulic pore radii.

From Eqs. (29) and (30) we have

$$\kappa_s = \frac{B_s \tau_s^2}{C_s} = \frac{\tau_s^2 L_h^2}{8C_s}. \tag{31}$$

Combining Eq. (10) with Eq. (31) then gives:

$$k = \kappa_s \phi_s = \frac{\tau_s^2 B_s \phi_s}{C_s} = \frac{\tau_s^2 L_h^2 \phi_s}{8C_s}. \tag{32}$$

We thus have a full description of the porous medium permeability by pore structure related parameters.

The permeability factor κ_s gives the effectiveness of the pore space Ω_s to conduct flow. This effectiveness is reduced by longer flow paths given with a smaller tortuosity τ_s, more variation in pore size along the flow paths described by a larger constriction factor C_s, and smaller pores reflected by a smaller characteristic length L_h. Note that these factors are dependent on direction in addition to the pore structure, which leads to the anisotropy of the permeability.

5 Single Tube Example

Capillary bundle of tubemodels have a wide use as simplified representations of porous media. The single tube examples in this section illustrate such model representations.

Consider a straight cylindrical tube with constant cross section of radius R. If the length of the tube is much larger than the radius, then the flow inside the tube is approximated by the Hagen–Poiseuille equation

$$Q = -\frac{\pi R^4 \rho g \nabla h}{8\mu}. \tag{33}$$

Moreover, the flow velocity is given by

$$u(r) = -\frac{(R^2 - r^2)\rho g \nabla h}{4\mu}, \tag{34}$$

where r is the distance from the center of the tube (Adler 1992). In the equation above and subsequently in this section, ∇h is also used to denote the scalar value $-\|\nabla h\|$. In the following subsections, the Hagen–Poiseuille equation is used to demonstrate our theory introduced above.

5.1 Permeability Factor

Consider a straight cylindrical tube inside a cube of side-length L, and with an applied piezometric head difference Δh over two opposite sides of the cube. Let the tube be of length L and aligned with the applied head, then the piezometric head gradient inside the tube is $\nabla h = \Delta h / L$.

Combining Darcy's law with the Hagen–Poiseuille equation, Eqs. (1) and (33), the permeability of the cube is given by:

$$k = -\frac{Q\mu L}{L^2 \rho g \Delta h} = \frac{\pi R^4}{8L^2}. \tag{35}$$

Using the flow velocity a distance r from the tube center as given by Eq. (34), and the piezometric head gradient $\nabla h = \Delta h / L$, the permeability factor described in Eq. (8) is $\kappa(r) = (R^2 - r^2)/4$. Taking the volume-weighted average then gives the effective permeability factor

$$\kappa_s = \frac{1}{\pi R^2 L} \int_0^L \int_0^R \kappa(r) 2\pi r \, dr \, ds = \frac{R^2}{8}. \tag{36}$$

This gives $\kappa_s \phi = \pi R^4/(8L^2)$, which is equal to the result from Darcy's law in Eq. (35), hence our results are consistent with Eq. (10).

5.2 Characteristic Length

Let our porous medium and applied piezometric head be as above. The permeability can be calculated using the individual contributions from the characteristic length, constriction, and tortuosity, as given by Eq. (32). The tortuosity and constriction are equal to 1 when the fluid flow inside the tube is described by the Hagen–Poiseuille equation, while the hydraulic conductance is $B(r) = (R^2 - r^2)/4$. The volume-weighted average of $B(r)$ is then equal to the integration of $\kappa(r)$ in Eq. (36), therefore, $B_s = R^2/8$. This gives a characteristic length

Fig. 1 Idealized porous medium with tortuosity different from 1
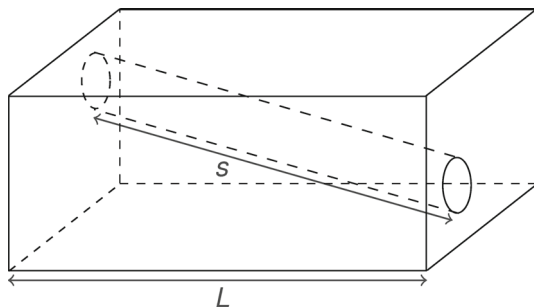
$L_h = \sqrt{8B_s} = R$. The characteristic length thus equals the radius of the tube, as desired. Since $\tau_s = 1$ and $C_s = 1$, we have

$$\frac{\tau_s^2 L_h^2 \phi}{8 C_s} = \frac{\pi R^4}{8 L^2}, \tag{37}$$

which agrees with the result from Darcy's law in Eq. (35), hence our results are consistent with Eq. (32).

5.3 Tortuosity

Let again our porous medium and applied piezometric head be as above, except that the length of the straight circular tube with constant cross-sectional area is $s > L$, as shown in Fig. 1. Then the piezometric head gradient inside the tube is $\nabla h = \Delta h / s$.

Combining Eqs. (1) and (33) gives the permeability as

$$k = -\frac{Q \mu L}{L^2 \rho g \Delta h} = \frac{\pi R^4}{8 L s}. \tag{38}$$

Note that a larger s gives a smaller permeability k, while $s = L$ gives a permeability equal to Eq. (35).

The calculations for the characteristic length in Sect. 5.2 still hold, so $L_h = R$. The constriction factor C_s is equal to 1, while each streamline has length s, thus $\tau_s = \tau(\mathcal{S}) = L/s$. We then have

$$\frac{\tau_s^2 L_h^2 \phi}{8 C_s} = \frac{\pi R^4}{8 L s}, \tag{39}$$

which is equal to the result from Darcy's law in Eq. (38), and consistent with Eq. (32).

Note that by changing the orientation of the tube shown in Fig. 1 the tortuosity and the permeability will change, while in this idealized case the characteristic length and constriction factor stay constant. In this case the anisotropy of the permeability is captured by the tortuosity.

5.4 Constriction

We will now use an idealized porous medium to investigate the effect of constriction. Consider a porous medium consisting of two tube segments in sequence aligned with the applied piezometric head, as depicted in Fig. 2. The two tube segments both have length $L/2$ inside a cube of side-length L, while the radii of the two segments are R_1 and R_2. When assuming $R_i \ll L/2$ for $i = 1, 2$, the flow inside the tube segments can be approximated by the Hagen–Poiseuille equations and the tortuosity can be approximated as $\tau_s = 1$.

Fig. 2 Idealized porous medium
with a single constriction
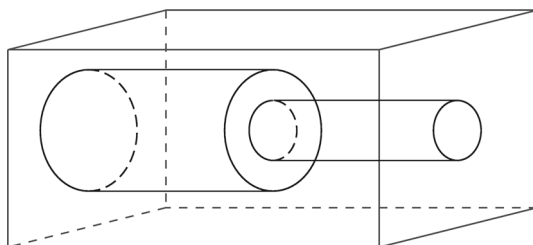
Invoking Eq. (33) we can show that the discharge is $Q = -(\pi R_1^4 R_2^4 \rho g \nabla h)/(4\mu(R_1^4 + R_2^4))$. Using Darcy's law, Eq. (1), we then obtain

$$k = -\frac{Q\mu L}{L^2 \rho g \Delta h} = \frac{\pi R_1^4 R_2^4}{4L^2(R_1^4 + R_2^4)}. \tag{40}$$

From Eq. (33) we have $\nabla h_i = -8\mu Q/(\pi R_i^4 \rho g)$, and from Eq. (21) we derive the constriction factor as

$$C_s = \frac{1}{L^2} \int_0^L \nabla h dx \int_0^L \frac{dx}{\nabla h} = \frac{1}{4} \frac{(R_1^4 + R_2^4)^2}{R_1^4 R_2^4}. \tag{41}$$

For each tube section we have $B_i = R_i^2/8$, which gives $B_s = (R_1^4 + R_2^4)/(8(R_1^2 + R_2^2))$. Since $\tau_s^2 = 1$, we have

$$k = \frac{\tau_s^2 B_s \phi_s}{C_s} = \frac{\pi R_1^4 R_2^4}{4L^2(R_1^4 + R_2^4)}, \tag{42}$$

consistent with Eq. (40). Note that a larger difference between R_1 and R_2 gives a larger constriction factor C_s, which then implies a lower permeability, while $C_s = 1$ when $R_1 = R_2$, as desired.

We will now revisit the more general constriction example from Sect. 3.2, where we considered a tube with cross-sectional area $A(x)$ for $x \in [0, L]$. We still assume that the flow inside the tube is approximated by the Hagen–Poiseuille equations and that the tortuosity can be approximated as $\tau_s = 1$. Then $\nabla h(x) = -8\mu Q\pi/(A(x)^2 \rho g)$, from Eq. (1) we then have

$$k = \frac{1}{8\pi L \int_0^L \frac{1}{A(x)^2} dx}. \tag{43}$$

The constriction factor

$$C_s = \frac{1}{L^2} \int_0^L \frac{1}{A(x)^2} dx \int_0^L A(x)^2 dx$$

equals Eq. (19) in Sect. 3.2. For the cross section at point x we have $B(x) = A(x)/(8\pi)$, thus $B_s = \int A(x)^2 dx/(8\pi \int A(x) dx)$.

Now assume another porous medium with equal pore volume and with a constant cross-sectional area. Then the cross-sectional area is $\hat{A} = (1/L) \int A(x) dx$, $\hat{B}_s = \hat{A}/(8\pi)$, and $\hat{k} = \hat{A}^2/(L^2 8\pi)$. When factoring out the hydraulic conductance, the reduction in permeability due to the varying cross-sectional area is
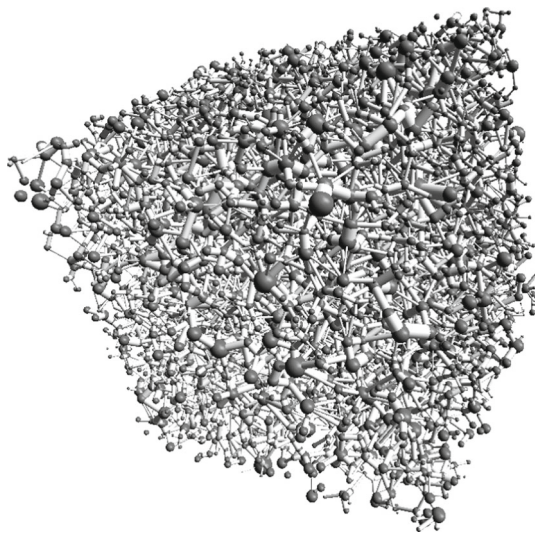
$$\frac{k/B_s}{\hat{k}/\hat{B}_s} = \frac{1}{C_s}, \tag{44}$$

hence the reduction equals the inverse of the constriction factor.

6 Fontainebleau Rock Example

We next turn to natural porous media, such as given by micro-CT (microtomography) images
and rock models of Fontainebleau sandstone. Using the e-Core software (E-Core 2012) we
generated three-dimensional rock models of Fontainebleau sandstone with porosities ranging
from 8 to 26 %. We used the exact same grain packing for all models, while we changed
the amount of quartz cementation to achieve the variation in porosities. The rock modeling
process is described in detail in Øren et al. (2006), Berg (2012). The micro-CT images and
model sample size were 2.7 mm cubed with a resolution of 5.7 µm.

We extracted network analogs using the e-Core software (E-Core 2012). The software
extracts a pore network using a grain-based algorithm (Bakke and Øren 1997), which seg-
ments the pore space into pore bodies and pore throats, each associated with a point $x \in V$,
a volume, a shape factor G (Mason and Morrow 1991), and an inscribed radius r (Patzek
and Silin 2001). One such network is visualized in Fig. 3. The distance between the two
pore bodies $t1$ and $t2$ connected by a pore throat $t3$ is divided into parts: parts l_{t1} and l_{t2} are
associated with each pore body, $t1$ and $t2$, respectively, and part l_{t3} is associated with the
pore throat.

Following Eq. (18) in Øren et al. (1998), the hydraulic conductance of each part is approx-
imated by

$$g = \frac{3r^4}{80\mu G}. \tag{45}$$

The effective hydraulic conductance between two pore bodies $t1$ and $t2$ connected by a pore
throat $t3$ is taken as the length-weighted harmonic average of the three parts

$$g_t = l_t \left(\frac{l_{t1}}{g_{t1}} + \frac{l_{t3}}{g_{t3}} + \frac{l_{t2}}{g_{t2}} \right)^{-1}, \tag{46}$$

Table 1 Micro-CT and model results

Rock	Porosity		Eff. Perm. fact. κ_s	Tortuosity		Const.	Characteristic length		Permeability	
	ϕ	ϕ_s	$[(\mu m)^2]$	τ_s	τ	C_s	L_h [μm]	r_c [μm]	$[(\mu m)^2]$	$[mD]$
mCTa	0.081	0.048	0.86	0.347	0.373	107.97	78.62	10.4	0.041	41.72
mCTb	0.128	0.114	4.569	0.41	0.425	28.41	78.5	15.1	0.521	528.06
mCTc	0.176	0.166	13.165	0.449	0.462	19.91	102.06	21.3	2.192	2220.86
mCTd	0.21	0.2	14.078	0.447	0.464	20.49	107.39	20.3	2.811	2848.57
a	0.086	0.056	0.766	0.337	0.355	105.3	75.28	9.1	0.043	43.44
b	0.101	0.079	1.865	0.363	0.381	58.97	81.73	13.2	0.147	149.22
c	0.125	0.111	3.841	0.387	0.405	40.51	91.08	15.3	0.427	432.61
d	0.153	0.143	9.573	0.431	0.451	26	103.6	18.8	1.371	1388.87
e	0.176	0.168	13.987	0.442	0.462	22.75	114.03	22.9	2.345	2376.21
f	0.206	0.198	22.428	0.461	0.48	18.36	124.6	26.3	4.449	4507.45
g	0.245	0.237	33.435	0.467	0.487	15.81	139.26	30.8	7.935	8040.4

where $l_t = l_{t1} + l_{t3} + l_{t2}$. Assuming a Hagen–Poiseuille type relation between the fluid discharge $Q_{t_{1,2}}$ from pore $t1$ to pore $t2$ and the head gradient $\nabla h_{t_{1,2}} = (h_{t2} - h_{t1})/l_t$ for each pore throat t, we have

$$Q_{t_{1,2}} = -g_t \frac{\rho g (h_{t2} - h_{t1})}{l_t}, \tag{47}$$

where h_{ti} is the piezometric head associated with the pore body ti.

The network model can now be viewed as a resistor network analog, with a one-to-one correspondence between the pore throats in the porous medium and the resistors in the resistor network analog, and also there is a one-to-one correspondence between the pore bodies and the network nodes. Each pore throat (resistor) t is given a conductance g_t/l_t. Let h_i be the piezometric head corresponding to pore body (node) i, and $\{t_{ij}\}_{j=1}^{\alpha_i}$ the pore throats (resistors) connected to pore body i. We then solve for h_i such that

$$\sum_{j=1}^{\alpha_i} -g_t \frac{\rho g (h_j - h_i)}{l_t} = \sum_{j=1}^{\alpha_i} Q_{t_{ij}} = 0, \tag{48}$$

where we have fixed piezometric head at the inlet and outlet boundaries.

The network volume with non-zero head gradient can be calculated as

$$\Omega_s = \sum_{h_{t1} \neq h_{t2}} \left(\frac{V_{t1}}{\alpha_{t1}} + \frac{V_{t2}}{\alpha_{t2}} + V_{t3} \right). \tag{49}$$

The values for porosity ϕ and $\phi_s = \Omega_s/V$ for the network representations of our micro-CT images and models are reported in Table 1. In Fig. 4 we have plotted porosity ϕ versus ϕ_s. A linear fit to the model data plotted in Fig. 4 gives the correspondence

$$\phi_s(\phi) = 1.126(\phi - 0.030). \tag{50}$$

The fluid velocity inside the network elements is not resolved; we therefore threat the fluid velocity as constant inside each network element. The average fluid velocity for part $t1$ and $t2$ is given by $u_{ti} = g_{ti} \rho g |h_{ti} - h_{it}| \alpha_{ti}/V_{ti}$ where $i = 1, 2$, while for part $t3$ it is $u_{t3} = g_{t3} \rho g |h_{1t} - h_{2t}|/V_{t3}$. Here h_{1t} and h_{2t} are piezometric heads such that $g_{t1} \rho g |h_{t1} -$

Fig. 4 Plot showing the correspondence between porosity ϕ and ϕ_s for the rock models and the micro-CT (mCT) data, together with a linear fit to the model data
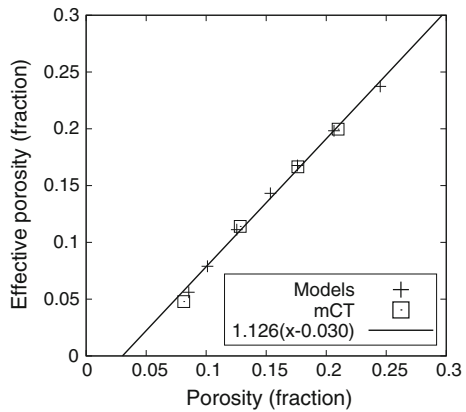
Fig. 5 Plot showing effective permeability factor κ_s versus porosity ϕ for the Fontainebleau rock models and the micro-CT (mCT) data, together with a fit to the data
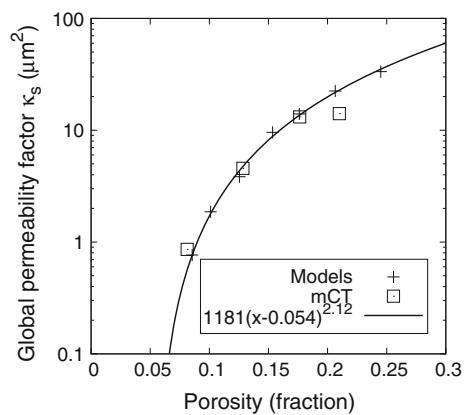
$h_{1t}|/l_{t1} = g_{t3}\rho g|h_{1t} - h_{2t}|/l_{t3} = g_{t2}\rho g|h_{2t} - h_{t2}|/l_{t2}$. The fluid velocity $\mathbf{u}$ is in the opposite direction of the gradient of the head, i.e., $\nabla h \cdot \mathbf{u} = -\|\nabla h\| u$. The local permeability factors for the sections t_1, t_2, t_3, as given by Eq. (8), are

$$\kappa_{ti} = \frac{g_{ti}(\rho g(h_{ti} - h_{it}))^2 \alpha_{ti}}{l_{ti} V_{ti}} \left(\frac{\Delta s}{\Delta h}\right)^2 \quad \text{for } i = 1, 2, \text{ and}$$

$$\kappa_{t3} = \frac{g_{t3}(\rho g(h_{1t} - h_{2t}))^2}{l_{t3} V_{t3}} \left(\frac{\Delta s}{\Delta h}\right)^2.$$

This enables the calculation of the effective permeability factor as the volume average of these local contributions:

$$\kappa_s = \frac{1}{\Omega_s} \sum_{h_{t1} \neq h_{t2}} \left(\frac{V_{t1}}{\alpha_{t1}}\kappa_{t1} + \frac{V_{t2}}{\alpha_{t2}}\kappa_{t2} + V_{t3}\kappa_{t3}\right). \tag{51}$$

The results are reported in Table 1.

The effective permeability factor κ_s versus porosity ϕ is plotted in Fig. 5. The function

$$\kappa_s(\phi) = 1181(\phi - 0.054)^{2.12}, \tag{52}$$

is included as a fit to the model data. For $\phi = 0.054$ we have $\kappa_s(\phi) = 0$, which is interpreted as percolation threshold for this sandstone (Mavko and Nur 1997).

Fig. 6 Plot showing porosity ϕ versus permeability k for the Fontainebleau rock models and micro-CT (mCT) data, together with Eq. (53) describing the correlation
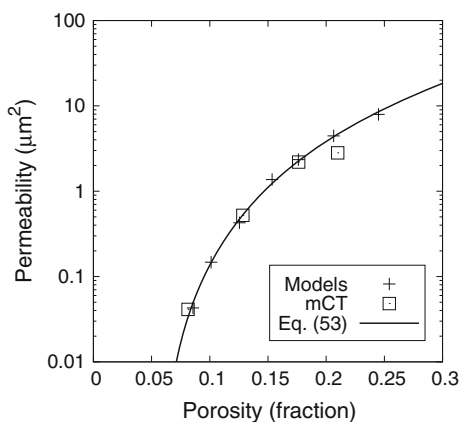
The permeability $k = \kappa_{\mathrm{s}}\phi_{\mathrm{s}}$, as given by Eq. (10), is also listed in Table 1. Calculated porosity and permeability for the network representations of Fontainebleau sandstone are plotted in Fig. 6. Combining Eqs. (10), (50) and (52), we have:

$$k(\phi) = \kappa_{\mathrm{s}}(\phi)\phi_{\mathrm{s}}(\phi) = 1181(\phi - 0.054)^{2.12}1.126(\phi - 0.030)$$
$$= 1329(\phi - 0.054)^{2.12}(\phi - 0.030). \tag{53}$$

This function is also included in Fig. 6 and provides a derived porosity-permeability relationship for the Fontainebleau samples.

We discretized the volume Ω_{s} into a disjoint union $\sqcup S$, where S is a subvolume of a single series of pore throats $t_S = \{t\}$, with the first throat connected to an inlet boundary and the last connected to an outlet boundary. Each S transports a constant discharge Q_S, and $\sum Q_S = Q$. The discretization $\sqcup S$ is a simplification of the streamlines, similar to the concept of a bundle of capillary tube model. In the network representation for the Fontainebleau sandstone the discretization $\Omega_{\mathrm{s}} = \sqcup S$ is dependent on the fluid flow across the network nodes; however, different ways of tracing streamlines across the network nodes were tested, yielding comparable results.

For the sections t_1, t_2 and t_3 of constant hydraulic conductance as associated with pore throat $t \in t_S$, we have the corresponding parts $\{S_{ti}\}$ of S. Each volume $S_{ti} \subset V_{ti}$ then has the associated length l_{ti}.

The three sections have

$$B_{ti} = -\frac{u}{\rho g \nabla h} = \frac{\mu g_{ti} l_{ti} \alpha_{ti}}{V_{ti}} \text{ for } i = 1, 2, \text{ and}$$

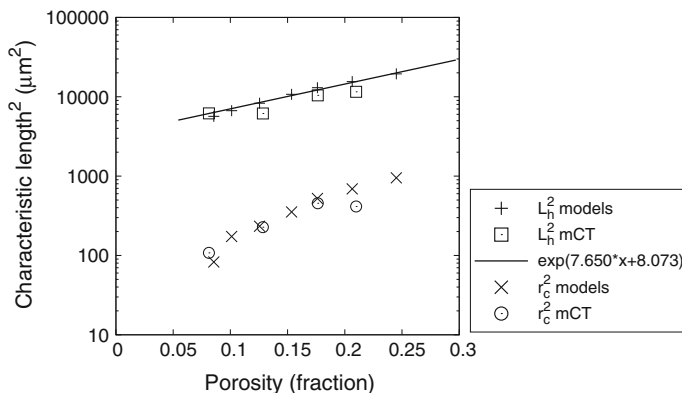$$B_{t3} = -\frac{u}{\rho g \nabla h} = \frac{\mu g_{t3} l_{t3}}{V_{t3}}.$$

For each S in $\Omega_s = \sqcup S$ we calculated

$$B(S) = \frac{1}{S} \sum_{t \in t_S} S_{t1} B_{t1} + S_{t2} B_{t2} + S_{t3} B_{t3}. \tag{54}$$

We separately calculated the constriction factor

$$C(S) = \frac{\Delta h}{\left(\sum_{t \in t_S} l_t\right)^2} \times \sum_{t \in t_S} \left(\frac{l_{t1}^2}{|h_{t1} - h_{1t}|} + \frac{l_{t2}^2}{|h_{t2} - h_{2t}|} + \frac{l_{t3}^2}{|h_{1t} - h_{2t}|}\right), \tag{55}$$

Fig. 7 Plot showing porosity ϕ versus characteristic length squared L_h^2 and critical pore radius squared r_c^2 for the Fontainebleau rock models and the micro-CT (mCT) data

and the tortuosity

$$\tau(\mathcal{S}) = \frac{\Delta s}{\sum_{t \in t_{\mathcal{S}}} l_t}. \tag{56}$$

We then obtain the characteristic length, constriction factor, and tortuosity for the volume Ω_s as

$$L_h = \sqrt{8B_s} = \sqrt{8 \frac{1}{\Omega_s} \sum \mathcal{S}B(\mathcal{S})}, \tag{57}$$

$$C_s = \frac{1}{Q} \sum Q_{\mathcal{S}} C(\mathcal{S}), \tag{58}$$

$$\tau_s^2 = \frac{1}{\sum \mathcal{S}B(\mathcal{S})} \sum \tau^2(\mathcal{S})\mathcal{S}B(\mathcal{S}). \tag{59}$$

The calculated values are reported in Table 1. We see that $\tau_s^2 L_h^2 / (8C_s) = \kappa_s$, which is consistent with Eq. (32).

For comparison we calculated the tortuosity τ as

$$\tau = \frac{\Delta s}{\frac{1}{Q} \sum_t Q_t l_t}, \tag{60}$$

where Q_t is the discharge through pore throat t (Bear 1988; Duda et al. 2011). Note that the values for τ_s and τ are similar; however, $\tau_s < \tau$. We also calculated the critical pore radius r_c corresponding to the smallest network element radius of the set of largest network elements that percolate through the network (Katz and Thompson 1986), where the radius of a network element is given by $r\sqrt[4]{3/(10G\pi)}$. The values are reported in Table 1. Such characteristic length scales are seen to be significantly lower than the hydraulic characteristic lengths L_h calculated according to Bear and Bachmat (1967), Bear (1988) for the Fontainebleau networks, included in Fig. 7.

In Fig. 7 we have plotted porosity ϕ versus the characteristic length squared L_h^2, the critical pore radius r_c, together with a functional fit $L_h^2(\phi) = \exp(7.650\phi + 8.073)$. For high porosities, i.e., rocks with little cementation and then larger pores, we have larger characteristic length L_h than for low porosities. The characteristic lengths L_h for the micro-CT images scatter around the trend given by the simulated rock models.
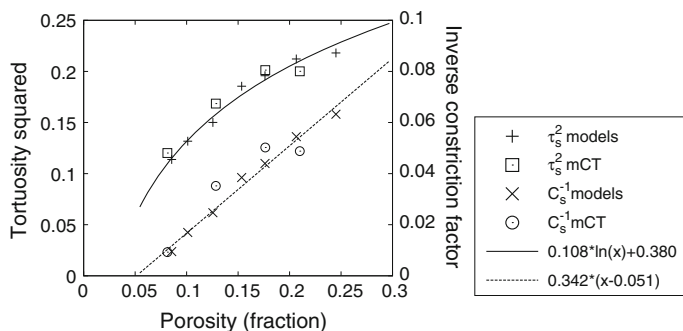
Fig. 8 Plot showing porosity ϕ versus both tortuosity squared τ_s^2 and inverse constriction C_s^- for the Fontainebleau rock models and the micro-CT (mCT) data

In Fig. 8 we have plotted porosity ϕ versus both the tortuosity τ_s^2 and the inverse constriction factor C_s^-. For high porosities we have less permeability reduction due to both tortuosity and constriction, compared to low porosities. Cementation increases the ratio between pore body and pore throat cross-sectional area, which yields a larger fluctuation in pore size along the streamlines and therefore a higher constriction factor. When cementation blocks pore throats completely, it increases the length of the streamlines and reduces the tortuosity τ_s.

A function $\tau_s^2(\phi) = 0.108 \ln(\phi) + 0.380$ gives a visual match to the tortuosity of the Fontainebleau sandstone models, while the constriction factor of the models follows a trend $C_s^-(\phi) = 0.342(\phi - 0.051)$. Both functions are also plotted in Fig. 8. The calculated tortuosity τ_s^2 and inverse constriction C_s^- of the micro-CT images follow the trend given by the models.

The calculated pore structure descriptors for each Fontainebleau sandstone sample reveal a strong functional relation with respect to porosity. This is desirable for sensitive descriptors. The functional trends display a non-trivial behavior at the percolation threshold derived in Eq. (52): The tortuosity τ_s^2 and characteristic length L_h^2 indicate a non-zero value at the percolation threshold, while the inverse constriction factor C_s^- tends to zero at the percolation threshold.

7 Conclusion

In this work we have fundamentally described and calculated the permeability in porous media. The permeability k of a porous medium is equal to $\kappa_s \phi_s$. Here the effective porosity ϕ_s is the fractional volume conducting flow from inlet to outlet. An effective permeability factor κ_s is given by the volume-weighted average of the microscopic permeability factors

$$\kappa = -\mu \rho g \nabla h \cdot \mathbf{u} \left(\frac{\Delta s}{\rho g \Delta h} \right)^2.$$

This microscopic permeability factor κ relates the local contribution of the pore structure to effectiveness of the pore space to conduct fluid flow κ_s.

We have shown that $\kappa_s = \tau_s^2 B_s / C_s = \tau_s^2 L_h^2 / (8 C_s)$, where the effective pore radius in the porous medium is described by the characteristic length L_h, fluctuation in local hydraulic radii is described by the constriction factor C_s, and the effective length of the streamlines is described by the tortuosity τ_s. These characteristic length, constriction factor, and tortuosity are direction dependent intrinsic descriptors of the pore structure. Their directional dependence leads to anisotropy of the permeability, i.e., the tensorial form of the permeability.

We have shown that our methodology reproduces results for Hagen–Poiseuille flow in tubes. It is also applied to a natural porous medium given by a pore network representation of Fontainebleau sandstone, where we show how the distinct contributions to the permeability from characteristic length, constriction, and tortuosity correlate with porosity. As long as the flow and piezometric head field can be obtained, this methodology is applicable to any porous medium.

This work demonstrates how the permeability can be related to porosity, in the sense of Kozeny–Carman, through fundamental and measurable descriptors of the pore structure. Such derived physical relation between permeability and porosity from detailed pore structure information leads to a better fundamental understanding of structure–property relations in porous media.

References

Adler, P.: Porous Media: Geometry and Transports. Butterworth-Heinemann, Stoneham (1992)

Adler, P., Jacquin, C., Quiblier, J.: Flow in simulated porous media. Int. J. Multiph. Flow **16**(4), 691–712 (1990)

Aris, R.: Vectors, Tensors and the Basic Equations of Fluid Mechanics. Dover publications, New York (1989)

Arns, C.H., Knackstedt, M.A., Pinczewski, M.V., Lindquist, W.: Accurate estimation of transport properties from microtomographic images. Geophys. Res. Lett. **28**(17), 3361–3364 (2001)

Bakke, S., Øren, P.: 3-d Pore-scale modelling of sandstones and flow simulations in the pore networks. SPE J. **2**(2), 136–149 (1997)

Banavar, J.R., Schwartz, L.M.: Magnetic resonance as a probe of permeability in porous media. Phys. Rev. Lett. **58**(14), 1411 (1987)

Bear, J.: Dynamics of fluids in porous media. Dover publications, New York (1988)

Bear, J., Bachmat, Y.: A generalized theory on hydrodynamic dispersion in porous media. In: IASH Symposium on Artificial Recharge and Management of Aquifers, vol. 72, pp. 7–16 (1967)

Berg, C.: Re-examining Archie's law: conductance description by tortuosity and constriction. Phys. Rev. E **86**, 046–314 (2012)

Berg, R.R.: Method for determining permeability from reservoir rock properties. Trans. Gulf Coast Assoc. Geol. Soc. **20**, 303–317 (1970)

Blunt, M.: Flow in porous media-pore-network models and multiphase flow. Current Opinion Colloid Interface Sci. **6**(3), 197–207 (2001)

Carman, P.: Fluid flow through granular beds. Trans. Inst. Chem. Eng. **15**, 150–166 (1937)

Darcy, H.: Dètermination des lois d'ècoulement de l'eau à travers le sable (1856). http://books.google.no/books?id=DOwbgyt_MzQC&printsec=frontcover#v=onepage&q&f=false

Duda, A., Koza, Z., Matyka, M.: Hydraulic tortuosity in arbitrary porous media flow. Phys. Rev. E **84**(3), 036–319 (2011)

Dullien, F.: Porous Media: Fluid Transport and Pore Structure. Academic press, San Diego (1992)

E-Core: v. 1.5.2. NumericalRocks, Software 2012

Fatt, I.: The network model of porous media. Trans. Am. Inst. Min. Metall. Pet. Eng. **207**, 144–181 (1956)

Guo, P.: Dependency of tortuosity and permeability of porous media on directional distribution of pore voids. Transport Porous Media **95**(2), 285–303 (2012)

Jiao, Y., Stillinger, F., Torquato, S.: A superior descriptor of random textures and its predictive capacity. In: Proceedings of the National Academy of Sciences, 106(42), 17634–17639 (2009)

Johnson, D.L., Koplik, J., Schwartz, L.M.: New pore-size parameter characterizing transport in porous media. Phys. Rev. Lett. **57**, 2564–2567 (1986)

Katz, A., Thompson, A.: Quantitative prediction of permeability in porous rock. Phys. Rev. B **34**(11), 8179–8181 (1986)

Koponen, A., Kataja, M., Timonen, J.: Tortuous flow in porous media. Phys. Rev. E **54**(1), 406 (1996)

Koponen, A., Kataja, M., Timonen, J.: Permeability and effective porosity of porous media. Phys. Rev. E **56**(3), 3319 (1997)

Kozeny, J.: Ueber kapillare leitung des wassers im boden. Wien Akad. Wiss **136**(2a), 271 (1927)

Lemaitre, R., Adler, P.: Fractal porous media iv: Three-dimensional stokes flow through random media and regular fractals. Transport Porous Media **5**(4), 325–340 (1990)

Mason, G., Morrow, N.R.: Capillary behavior of a perfectly wetting liquid in irregular triangular tubes. J. Colloid Interface Sci. **141**(1), 262–274 (1991)

Mavko, G., Nur, A.: The effect of a percolation threshold in the Kozeny–Carman relation. Geophysics **62**, 1480 (1997)

Mostaghimi, P., Blunt, M.J., Bijeljic, B.: Computations of absolute permeability on micro-ct images. Math. Geosci. **45**(1), 103–125 (2013)

Øren, P., Bakke, S., Arntzen, O.: Extending predictive capabilities to network models. SPE J. **3**(4), 324–336 (1998)

Øren, P., Bakke, S., Rueslåtten, H.: Digital core laboratory: rock and flow properties derived from computer generated rocks. In: Proceedings of the Annual Symposium of the Society of Core Analysts (2006)

Øren, P.E., Bakke, S.: Process based reconstruction of sandstones and prediction of transport properties. Transport Porous Media **46**(2–3), 311–343 (2002)

Patzek, T., Silin, D.: Shape factor and hydraulic conductance in noncircular capillaries: I. One-phase creeping flow. J. Colloid Interface Sci. **236**(2), 295–304 (2001)

Saeger, R., Scriven, L., Davis, H.: Flow, conduction, and a characteristic length in periodic bicontinuous porous media. Phys. Rev. A **44**(8), 5087 (1991)

Schopper, J.: A theoretical investigation on the formation factor/permeability/porosity relationship using a network model. Geophys. Prospect. **14**(3), 301–341 (1966)

Schwartz, L., Auzerais, F., Dunsmuir, J., Martys, N., Bentz, D., Torquato, S.: Transport and diffusion in three-dimensional composite media. Phys. A **207**(1), 28–36 (1994)

Schwartz, L., Martys, N., Bentz, D., Garboczi, E., Torquato, S.: Cross-property relations and permeability estimation in model porous media. Phys. Rev. E **48**(6), 4584 (1993)

Van Brakel, J., Heertjes, P.: Analysis of diffusion in macroporous media in terms of a porosity, a tortuosity and a constrictivity factor. Int. J. Heat Mass Transf. **17**(9), 1093–1103 (1974)

Yeong, C., Torquato, S.: Reconstructing random media. ii. Three-dimensional media from two-dimensional cuts. Phys. Rev. E **58**(1), 224 (1998)

Zhang, X., Knackstedt, M.A.: Direct simulation of electrical and hydraulic tortuosity in porous solids. Geophys. Res. Lett. **22**(17), 2333–2336 (1995)